Human Rad52 binds and wraps single-stranded DNA and mediates annealing via two hRad52–ssDNA complexes

Jill M. Grimme[1,2], Masayoshi Honda[1], Rebecca Wright[1], Yusuke Okuno[1], Eli Rothenberg[3], Alexander V. Mazin[4], Taekjip Ha[3,5,6] and Maria Spies[1,3,6,*]

[1]Department of Biochemistry, University of Illinois at Urbana-Champaign, Urbana, IL 61801, [2]US Army Corps of Engineers, Construction Engineering Research Laboratory, Champaign, IL, 61822, [3]Howard Hughes Medical Institute, Urbana, IL 61801, [4]Department of Biochemistry and Molecular Biology, Drexel University College of Medicine, Philadelphia, PA 19102-1192, [5]Department of Physics and [6]Center for Biophysics and Computational Biology, University of Illinois at Urbana-Champaign, Urbana, IL 61801, USA

ABSTRACT

Rad52 promotes the annealing of complementary strands of DNA bound by replication protein A (RPA) during discrete repair pathways. Here, we used a fluorescence resonance energy transfer (FRET) between two fluorescent dyes incorporated into DNA substrates to probe the mechanism by which human Rad52 (hRad52) interacts with and mediates annealing of ssDNA–hRPA complexes. Human Rad52 bound ssDNA or ssDNA–hRPA complex in two, concentration-dependent modes. At low hRad52 concentrations, ssDNA was wrapped around the circumference of the protein ring, while at higher protein concentrations, ssDNA was stretched between multiple hRad52 rings. Annealing by hRad52 occurred most efficiently when each complementary DNA strand or each ssDNA–hRPA complex was bound by hRad52 in a wrapped configuration, suggesting homology search and annealing occur via two hRad52–ssDNA complexes. In contrast to the wild type protein, hRad52^RQK/AAA and hRad52^1−212 mutants with impaired ability to bind hRPA protein competed with hRPA for binding to ssDNA and failed to counteract hRPA-mediated duplex destabilization highlighting the importance of hRad52-hRPA interactions in promoting efficient DNA annealing.

INTRODUCTION

The eukaryotic Rad52 recombination mediator protein participates in maintenance of genomic integrity by functioning in homologous recombination (HR), homology-directed DNA repair (HDR), and rescue of collapsed replication forks (1–4). The importance of Rad52 is underscored by the high sequence conservation in all eukaryotes (5–9). *In vitro* biochemical investigations also suggest strong functional conservation. Rad52 proteins from yeast and vertebrates share two characteristic activities: (i) they facilitate replacement of RPA bound to ssDNA with Rad51 (or Dmc1) and therefore assist in the formation of Rad51 (or Dmc1) nucleoprotein filaments, which are the active species during homology search and strand exchange steps of HR and HDR (10–13); and (ii) they promote annealing of complementary DNA strands as well as annealing between ssDNA–RPA complexes (14,15). Similar to that of its yeast counterpart, the strand annealing activity of hRad52 plays a role in HR, which is a vital mechanism for repair of the deleterious DNA double-strand breaks (DSB) because it confers the highest fidelity of repair (16). In both, classical DNA double-stranded break repair (DSBR) and synthesis dependent strand annealing (SDSA) models annealing between two long complementary ssDNA regions represents an important step in recombinational DNA repair (17–22). In contrast, annealing of relatively short homologous sequences [as short as 29 bp in length (23)] located in the vicinity of a DNA break is a prerequisite of the single-strand annealing (SSA) mechanism of HDR.

*To whom correspondence should be addressed. Tel: +1 217 244 9493; Fax: +1 217 244 5858; Email: mspies@life.illinois.edu

The authors wish it to be known that, in their opinion, the first two authors should be regarded as joint First Authors.

The large representation of repeats in the human genome (24) makes SSA an important pathway for both DNA repair and mutagenesis (25).

Because of its crucial role in HR and DNA repair, yeast Rad52 has been the subject of comprehensive genetic and biochemical analyses (26). In contrast to the severe recombination and repair phenotypes observed in yeast, inactivation of *RAD52* only mildly affects recombination in vertebrates (27–29). Vertebrates have a number of genes encoding proteins that possess functions complementary to Rad52 activities. Activities of these proteins, therefore, may obscure Rad52 importance. It is also possible that despite being homologs, yeast and vertebrate Rad52 proteins may in fact have quite distinct *in vivo* functions. Characterization of human Rad52 has encompassed *in vitro* analyses of its role in facilitating Rad51 nucleoprotein filament formation as well as its annealing ability (10,20,30–32). Structural investigations of Rad52 revealed ring-shaped oligomers for both yeast and human proteins with the predominant form being a heptamer (33,34). Two high resolution structures were obtained for a truncated hRad52 consisting of the conserved ssDNA annealing domain (35,36). The diameter of the undecameric ring for the truncated protein, despite additional subunits, is no larger than the heptameric ring for the full-length protein. Therefore, the overall subunit arrangement within the undecameric ring of the truncated protein is believed to accurately represent the arrangement within the heptameric ring of the full-length protein. Although both structures were obtained without DNA, a positively charged groove along the outer surface of the Rad52 ring is the predicted DNA-binding site. In addition, a secondary DNA-binding site was recently identified within the conserved N-terminal domain of hRad52 protein (37).

The ring-shaped oligomeric structure with the DNA-binding site spanning its perimeter might be important for the mediator function: hexameric UvsY, a Rad52 functional homolog from bacteriophage T4, binds ssDNA as well as complexes comprised of by ssDNA and gp32, which is the functional equivalent of eukaryotic RPA protein, in a wrapped configuration and this binding mode is critical for UvsY-mediated formation and stabilization of UvsX (RecA/Rad51 homolog) nucleoprotein filaments (38).

Despite the wealth of information uncovered in previous investigations, the mechanistic aspects of hRad52–ssDNA interactions remained unresolved. In particular, it is unclear what species participate in hRad52-mediated annealing. Inhibition of DNA annealing in gel-based assays by high concentrations of hRad52 (30) may be viewed as evidence that annealing mainly occurs between a hRad52–ssDNA complex and a protein-free DNA, or between one strand in complex with hRad52 and another bound by hRPA given the copious amounts of hRPA used in typical assays and those found in the cell.

Here, we developed FRET-based binding and annealing assays to resolve the DNA-binding mode of hRad52 and to identify what hRad52–hRPA–ssDNA complexes are responsible for efficient annealing. We used the full-length hRad52 and a truncation mutant, hRad52$^{1-212}$, which is comprised of only the N-terminal half of the protein that contains both the primary and secondary DNA-binding sites and lacks the protein-protein interaction regions for hRad51 and hRPA. We also constructed a full-length hRad52 mutant protein (designated as hRad52$^{RQK/AAA}$) which has impaired interaction with hRPA. Our results revealed that ssDNA can be wrapped around the hRad52 ring, but multiple rings can bind one ssDNA molecule at elevated hRad52 concentrations. These two distinct binding modes affected the rate and extent of annealing differentially. The highest annealing rate was achieved at protein concentrations where each DNA strand was in a complex with a hRad52 protein ring. In contrast, higher order hRad52–ssDNA complexes impeded annealing. Similar results were obtained for the full-length hRad52 protein when presented with ssDNA bound by hRPA, except that the extent and the rate of annealing were reduced likely as a result of competition between hRad52-mediated annealing and hRPA-mediated duplex destabilization. Notably, hRPA effectively competed for binding to ssDNA with hRad52$^{1-212}$ and hRad52$^{RQK/AAA}$ and inhibited annealing mediated by these proteins. Therefore, both the wrapped conformation of ssDNA strands and the physical interaction between hRad52 and hRPA were required for efficient annealing of hRPA coated ssDNA molecules.

MATERIALS AND METHODS

Materials

All Cy3- or Cy5-labeled DNA substrates (HPLC purified) were purchased from Integrated DNA Technologies (Coralville, IA). All chemicals were reagent grade.

Expression vectors for hRad52$^{RQK/AAA}$ and hRad52$^{1-212}$ mutants

The pET15b-6HIS-hRAD52 plasmid (39) was used as template for construction of the RPA-binding deficient and C-terminal truncation mutants of hRad52 protein. We used a QuikChange II XL site-directed mutagenesis kit (Stratagene) and the following primers 5′hR52 261-263 RQK/AAA (5′-CGCACCAGCGGAAGCTCGCGGCAGCTC-AGCTGCAGCAGCAGTTCC-3′) and 3′hR 261-263 RQK/AAA (5′-GGAACTGCTG-CTGCAGCTGAGCTGCCGCGAGCTTCCGCTGGTGCG-3′) to achieve the following substitutions: R261A, Q262A, and K263A. We used the same kit and the 5′hR52 1-212 (5′-TGCCGACCGAACATGTAATAATAAGCCCTGGGACAC C-3′) and 3′hR52 1-212 (5′- GGTGTCCCAGGGCTTATTATTACATGTTCGGTCGG CA-3′) primers to introduce three stop codons (TAA) at the end of the coding sequence for the first 212 amino acids of hRad52. Successful construction of the pET15b-6HIS-hRAD52$^{RQK/AAA}$ and the pET15b-6HIS-hRAD52$^{1-212}$ plasmids was confirmed by sequencing (DNA Core Sequencing Facility, UIUC).

Proteins

Human RPA protein was expressed and purified as previously described (40).

Human Rad52, hRad52$^{RQK/AAA}$ and Rad52$^{1-212}$ proteins were purified essentially as described for full-length hRad52 (10,32). The concentrations of each protein were determined using their extinction coefficients: $40\,380\,M^{-1}\,cm^{-1}$ (hRad52 and hRad52$^{RQK/AAA}$), $20\,775\,M^{-1}\,cm^{-1}$ (hRad52$^{1-212}$) and $84\,000\,M^{-1}\,cm^{-1}$ (hRPA).

FRET-based DNA binding and annealing assays

FRET-based analyses of DNA binding by full-length hRad52, hRad52$^{RQK/AAA}$ or hRad52$^{1-212}$ proteins were carried out using a Cary Eclipse fluorescence spectrophotometer (Varian) at 25°C in buffer containing 30 mM Tris–Acetate (pH 7.5) and 1 mM DTT. Measurements began with buffer only (baseline) followed by addition of the respective DNA substrate (1 nM unless indicated otherwise) dually labeled with Cy3 and Cy5 fluorophores. Following Cy3 excitation at 530 nm, the emission of the acceptor Cy5 and donor Cy3 fluorophores were monitored simultaneously at 660 and 565 nm, respectively. The FRET efficiency (E_{FRET}) was calculated as:

$$E_{FRET} = \frac{4.2 {}^* I_{Cy5}}{4.2 {}^* I_{Cy5} + 1.7 {}^* I_{Cy3}},$$

where I_{Cy5} is the averaged acceptor intensity and I_{Cy3} is the averaged donor intensity. The I_A and I_D values were calculated by averaging the measured fluorescence intensities for each dye over 2 min after the signal had equilibrated and subtracting the background fluorescence. The correction factors (4.2 for the Cy3 dyes and 1.7 for the Cy5 dye) were assigned based on the fraction of the donor fluorescence in the acceptor channel and the fraction of acceptor fluorescence in the donor channel, respectively specific to our instrument. After the signal for DNA alone was recorded, hRad52, hRad52$^{RQK/AAA}$ or hRad52$^{1-212}$ was titrated into the reaction mixtures. The fluorescence of the donor and the acceptor was recorded as above. The calculated E_{FRET} was plotted against the hRad52, hRad52$^{RQK/AAA}$ or hRad52$^{1-212}$ concentrations (in monomers) using GraphPad Prism4 software.

Binding of the hRad52, hRad52$^{RQK/AAA}$ or hRad52$^{1-212}$ to the Cy3-Cy5 labeled ssDNA substrates was also monitored in the presence of hRPA protein. The assays were carried out as described above with the 2 nM hRPA incubated with ssDNA for 3 min before the first addition of hRad52, hRad52$^{RQK/AAA}$ or hRad52$^{1-212}$.

Annealing of complementary oligonucleotides by hRad52, hRad52$^{RQK/AAA}$ or hRad52$^{1-212}$ was monitored under similar conditions as the binding assays. The DNA substrates used were a 'target' molecule 28 nt in length (T-28) with Cy3 incorporated at the center (5′-ATAGTT ATGGTGAGGACCC/**iCy3**/CTTTGTTTC-3′) and a Cy5-labeled complementary 'probe' molecule (5′-GAAA CAAAGGGGTCC/**iCy5**/ TCACCATAACTAT-3′) (P-28). When annealed, the Cy3 and Cy5 dyes were separated by 5–6 nt yielding a high FRET signal

(0.81 under our experimental conditions). To carry out FRET measurements between non-complementary strands we used T-28 and P′-28 oligonucleotides, where P′-28 sequence (5′-ATAGTTATGGTGAGGACCC/**iCy5**/CTTTGTTTC-3′) was identical to that of T-28. For each assay, the reaction master mixture containing the indicated concentrations of proteins (hRad52, hRad52$^{RQK/AAA}$, hRad52$^{1-212}$ and/or hRPA) was prepared at room temperature and divided into two half-reactions. Following the baseline (buffer and proteins) measurement, 0.5 nM of Cy3-labeled target ssDNA substrate was added to the reaction cuvette, and the signal was allowed to stabilize. The annealing reaction was initiated upon addition of the second half-reaction pre-incubated with 0.5 nM Cy5-labeled probe ssDNA. The fluorescence of Cy3 and Cy5 were measured simultaneously over the reaction time course (400 s). The change in E_{FRET} was calculated by averaging the E_{FRET} value for three independent annealing reactions for each protein concentration tested. This averaged E_{FRET} was plotted against time and fitted to a double exponential whose combined amplitude was compared to E_{FRET} value for dsDNA (0.81) and fully ssDNA (0.18 as determined by mixing two heterologous Cy3- and Cy5-labeled oligonucleotides in the absence of proteins or by mixing the T-28 and P-28 molecules bound by 2 nM hRPA) to determine the extent of annealing reaction. The initial rate of annealing was determined as the slope of the linear portion of the progress curve (5–20 s depending on the protein concentration) for each assay, divided by 0.63 (E_{FRET} difference between fully single-stranded and fully annealed DNA) and multiplied by the total amount of dsDNA present (0.5 nM). The error bars are the standard error for the slope of the line. Both the rate and extent of annealing were plotted against the hRad52, hRad52$^{RQK/AAA}$ or hRad52$^{1-212}$ protein concentration and analyzed using GraphPad Prism4 software.

Gel-based DNA-binding assays

The Cy3-Cy5 labeled 30 or 60 mer poly(dT) oligonucleotide (50 nM) was mixed with hRad52 (175, 350, 525, 700, 875 and 1050 nM) in 10 μl of standard reaction buffer, containing 30 mM Tris–Acetate (pH 7.5) and 1 mM DTT. The reaction mixtures were incubated at 37°C for 10 min, fixed with 0.1% glutaraldehyde and were analyzed by non-denaturing 3.5% polyacrylamide electrophoresis in TBE buffer (90 mM Tris, 64.6 mM boric acid and 2 mM EDTA [pH 8.0]). The signals were visualized using a Storm 9600 fluorescence imager (GE Healthcare) by exciting and visualizing Cy5 fluorescence, and analyzed using ImageQuant software.

Polyhistidine-tag pulldown assays

The pull-down assays were performed in 50 μl reactions containing 30 mM Tris–Acetate [pH 7.5], 50 mM KCl, 20 mM imidazole, 1 mM DTT and 0.2% (vol/vol) Triton X-100. hRad52, hRad52$^{RQK/AAA}$ and hRad52$^{1-212}$ (5 μM) were incubated with 5 μM hRPA for 20 min at 4°C. An equal volume (50 μl) of Ni-NTA magnetic agarose beads

(QIAGEN) was washed with 100 µl of reaction buffer and added to the reaction. After the incubation and magnetic separation of the beads, supernatant was removed from the reaction for the unbound samples. The beads were washed twice with 200 µl of reaction buffer and re-suspended in 50 µl of elution buffer (30 mM Tris–acetate [pH 7.5], 300 mM imidazole, 1 mM DTT, 0.1% SDS). The unbound and eluted fractions were subjected to 12.5% SDS–PAGE gel electrophoresis followed by Coomassie Brilliant Blue staining.

RESULTS

Human Rad52 protein displays two modes of ssDNA binding

Structures of the highly conserved DNA annealing domain of hRad52 protein (35,36) combined with genetic analyses (14,41) suggest that the primary DNA-binding site of human Rad52 involves the positively charged groove on the outer surface of the hRad52 ring. The location and continuity of the DNA-binding site predicted that ssDNA may wrap around the perimeter of the protein ring, but this prediction has not been directly tested and alternative binding modes for hRad52 can be envisioned (42,43). Residues constituting the secondary DNA-binding site are located on the 'top' of the hRad52 ring above the positively charge groove designated as primary ssDNA-binding site (37). It is unclear how the DNA is distributed between the two sites during the annealing process. Moreover, estimates of the Rad52 affinity for ssDNA range from sub-nM to 100 nM (41,44,45). Therefore, we carried out FRET-based DNA-binding experiments to establish the DNA-binding mode of hRad52 and to quantitatively evaluate its equilibrium binding to ssDNA.

If ssDNA binding occurs as proposed, then wrapping of an oligonucleotide of a length similar to the circumference of the hRad52 ring, labeled with a donor fluorophore on one terminus and with an acceptor fluorophore on the other, should yield much higher FRET in hRad52–ssDNA complex relative to the protein-free ssDNA. Each subunit of the hRad52 heptamer accommodates 4 nt of ssDNA (46). Therefore, we expected to see the most pronounced change in FRET for ssDNA close to 28 nt in length.

Cartoon in Figure 1A (blue box) illustrates possible binding configurations consistent with calculated FRET efficiency (E_{FRET}) of the 30-nt long poly(dT) ssDNA substrate (1 nM), labeled with the donor (Cy3) at the 3′ end and the acceptor (Cy5) at the 5′ end, as a function of the hRad52 monomer concentration (blue curve in Figure 1B). At sub-saturating concentrations, hRad52 readily bound to the poly(dT)-30 substrate resulting in a linear increase in FRET with increasing protein concentration (High FRET phase). We attributed this increase in FRET to the growing fraction of ssDNA molecules wrapped around the hRad52 ring. The highest E_{FRET} was achieved for the poly(dT)-30 substrate at approximately stoichiometric amounts of DNA (1 nM) to hRad52 monomer (8 nM) as shown in blue dashed

line in the inset of Figure 1B. Further increase in the hRad52 concentration resulted in a decrease in E_{FRET}, which represents the unwrapping of the ssDNA and may be attributed to the binding of multiple hRad52 oligomers to the same DNA molecule (medium FRET phase). We also monitored protein concentration dependence of the FRET signal originated from the mixture of non-complementary Cy3- and Cy5-labeled oligonucleotides T-28 and P′-28 (red box in Figure 1A and red curve in Figure 1B). Increase in E_{FRET} in these experiments can be attributed to two heterologous oligonucleotides bound to the same hRad52 oligomer or bound to two different but interacting hRad52 rings. In either case, two ssDNA molecules would be brought sufficiently close to each other as would be expected to happen during homology search and DNA annealing. Indeed, E_{FRET} between donor and acceptor fluorophores present on different heterologous ssDNA molecules increased in the hRad52 concentration dependent manner (medium FRET phase). The maximal E_{FRET} amplitude was achieved at 6–7 nM of hRad52 (red dashed line in the inset of Figure 1B), which is only slightly below the stoichiometric ratio of hRad52 and ssDNA (7 nM, which corresponds to 4 nt of ssDNA per one monomer of hRad52 or one heptameric ring per one ssDNA molecule). Considering that at the stoichiometric condition we expect most hRad51/ssDNA species to contain one 30-mer oligonucleotide bound in wrapped configuration per one hRad52 ring, there may be frequent and transient ssDNA–ssDNA interaction between two ssDNA–hRad52 rings, resulting in the observed medium FRET signal.

The electrophoretic mobility shift assays (Figure 1C) confirmed our interpretation of the FRET data: the highest amount of band shift corresponding to a single Rad52 heptamer ring bound to ssDNA was observed at the stoichiometric concentrations of hRad52 and DNA (seven monomers per one 30-nt long ssDNA molecule, lane 3). In high concentration of Rad52, multiple Rad52 ring binding to ssDNA make high molecular weight Rad52–ssDNA aggregation (lanes 6 and 7). This multiple Rad52 and ssDNA complex formation made Cy3 and Cy5 labeled heterologous DNA spatially separated and prevent free DNA–DNA interaction as shown in significantly reduced E_{FRET} (low FRET phase).

The longer poly(dT)-60 substrate, with internally placed fluorophores separated by 25 nt (Figure 1D), exhibited a trend in calculated E_{FRET} comparable to that observed for dually labeled poly(dT)-30 (Figure 1E). However, higher concentration (15 nM) of hRad52 was required to reach maximal E_{FRET} (blue dashed line in the inset of Figure 1E) indicating that in contrast to poly(dT)-30, poly(dT)-60 can accommodate two hRad52 oligomers in a wrapped configuration corresponding to maximal E_{FRET} (Figure 1D, High FRET phase). Only the hRad52 oligomer bound to the 5′ half of the poly(dT)-60 where the dyes are located will contribute to the FRET signal, and the highest E_{FRET} value is achieved when two hRad52 rings are bound to the same substrate. Higher concentrations of hRad52 resulted in a decrease in E_{FRET} again suggesting the binding of
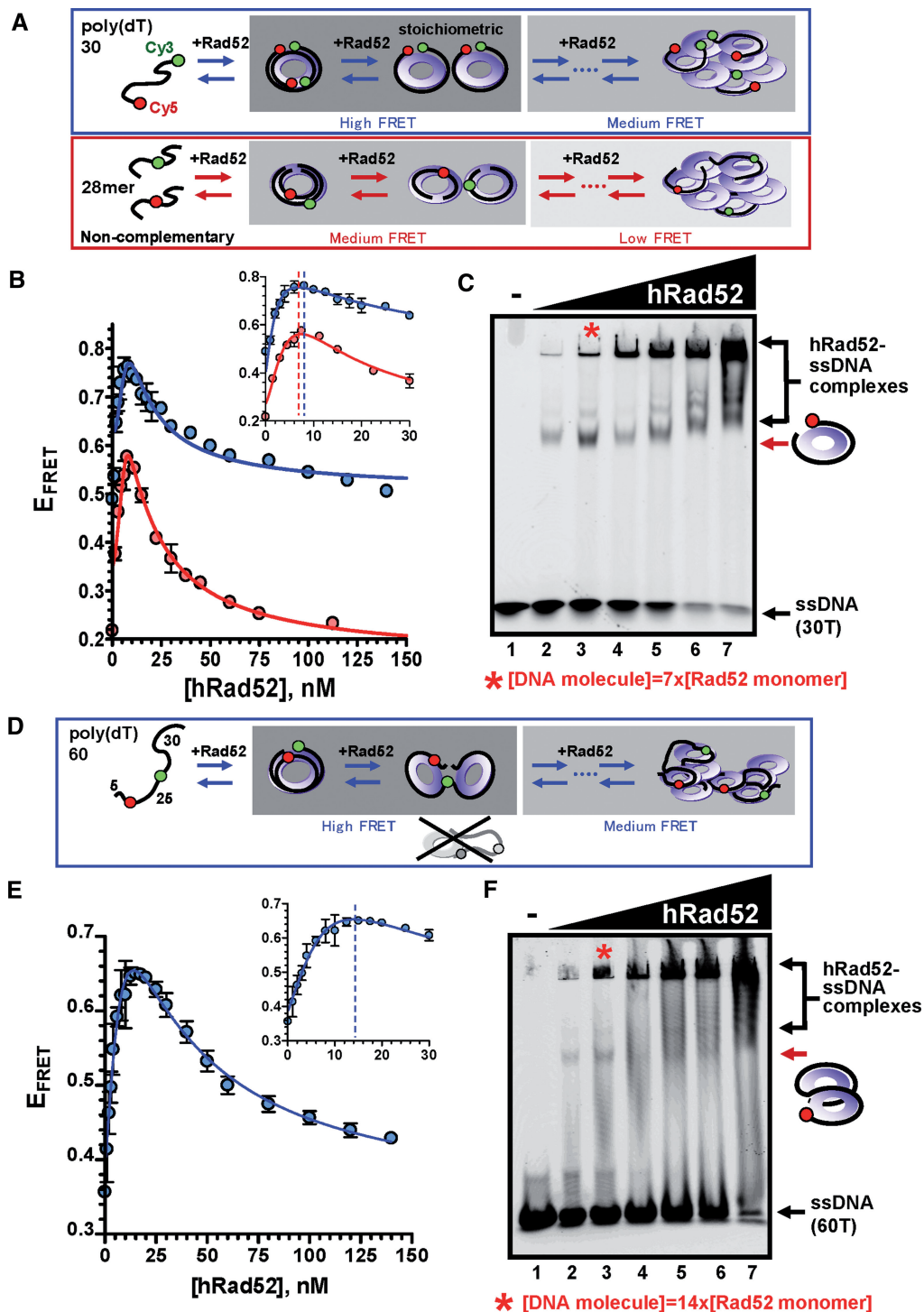
Figure 1. hRad52 displays a bi-phasic ssDNA binding behavior. FRET and gel-based ssDNA-binding assays with hRad52. The poly(dT)-30 and poly(dT)-60 substrates were end-labeled with the donor Cy3 (green) and acceptor Cy5 (red) fluorescent dyes. The two heterologous 28-mer oligonucleotides were internally labeled with Cy3 and Cy5 dyes, respectively. (**A**) Cartoon interpretation for the observed FRET states for experiments using dually labeled poly(dT)-30 (blue box) and two heterologous oligonucleotides (red box). Blue circles depict projections of hRad52 heptameric rings with primary and secondary DNA-binding site aligned inside the ring (not depicted separately). (**B**) Titrations were performed by additions of hRad52 at indicated concentrations to a solution containing 1 nM poly(dT)-30 ssDNA (blue curve) or 0.5 nM each Cy3- and Cy5-labeled 28-mers (1 nM total; red curve). The data points and error bars represent averages and standard deviations for three independent titrations. (**C**) The dually-labeled poly(dT)-30 substrates (50 nM molecules) were also used in gel-based DNA-binding assays as described in the materials and methods. The respective positions of the protein ssDNA and various mobility-shifted complexes are indicated by arrows on the right of the gel. Red asterisk marks stoichiometric-binding condition where seven monomers of hRad52 are present per one 30-mer ssDNA. (D) Cartoon representation of possible poly(dT)-60-hRad52 complexes and corresponding FRET states. (E) Internal positions of Cy3 and Cy5 in the longer ssDNA poly(dT)-60 demonstrate a wrapped conformation of ssDNA around the perimeter of the hRad52 ring because the peak FRET could not be achieved by hRad52 binding only to the ends of ssDNA (grey complex). (**F**) Mobility-shift assay carried out with 50 nM poly(dT)-60 ssDNA. Red asterisk marks stoichiometric concentration.

multiple protein oligomers (medium FRET phase). Importantly, the bi-phasic hRad52-binding isotherms in the presence of poly(dT)-60, in which the donor and acceptor dyes are positioned internally, demonstrated that the observed FRET change resulted from DNA continuously wrapped around the hRad52 rings and not from hRad52 capturing only the ends of the labeled strands (Figure 1D, grey complex). If the latter were true, we should have observed no increase in E_{FRET} associated with phase I for this substrate.

As with the shorter substrate, the electrophoretic mobility shift assays (Figure 1F) confirmed the FRET data interpretations: the longer poly(dT)-60 substrate can accommodate two hRad52 oligomers in a wrapped conformation at stoichiometric concentrations of hRad52 and DNA (lane 3). We also observed high molecular weight hRad52-ssDNA aggregation at higher hRad52 concentrations (lanes 6 and 7) as with the shorter poly(dT)-30 substrate.

Additional binding mode comparisons were performed with end-labeled poly(dT)-22, poly(dT)-39 and poly(dT)-50 (Supplementary Figure S1). A similar binding trend was displayed for these substrates. The highest E_{FRET} for the poly(dT)-39 and poly(dT)-50 was achieved at the protein concentrations similar to that required to wrap the poly(dT)-60 substrate, suggesting that 39-mer ssDNA may accommodate more than one oligomeric ring. In contrast, poly(dT)-22 required the same concentration of protein to achieve maximal E_{FRET} as poly(dT)-30. Due to the shorter distance between the two ends, the change in the FRET signal was lower for this substrate (Supplementary Figure S1).

Based on the bi-phasic shape of the binding curves described above, we propose that binding in the wrapped mode at low hRad52 concentrations is very tight ($K_d \ll 1\,nM$) so that hRad52 forms stoichiometric complexes with ssDNA, supporting subnanomolar affinity of hRad52 for ssDNA determined by others (44). In the second, extended binding mode, not all protomers within the hRad52 rings are bound to ssDNA resulting in a lower affinity interaction and therefore in a distinguishable phase on the binding curve. To confirm stoichiometric binding, FRET-based-binding assays for hRad52, were performed for a range of DNA concentrations (1, 2 and 10 nM). As expected, at higher the DNA concentration, more hRad52 was needed to reach maximum E_{FRET} (Supplementary Figure S2).

Human Rad52 bound dsDNA, end-labeled with Cy3 and Cy5 dyes on opposite termini of the 30-nt strands, in a bent conformation (Supplementary Figure S3). Although the initial FRET was lower for dsDNA due to the increased rigidity of the double helix, the correlation of the E_{FRET} trends for ssDNA and dsDNA indicated similar DNA distortion by hRad52. It is likely that this dsDNA distortion is caused by binding into the secondary DNA-binding site located on the top of the hRad52 ring (37), which in contrast to the narrow groove of primary DNA-binding site should present no steric hindrance to duplex binding.

$R^{261}Q^{262}K^{263}$ in the C-terminal region of hRad52 are responsible for hRad52–RPA interaction

Replication protein A (RPA) plays critical roles in DNA replication, recombination and repair. Importantly, RPA interacts with Rad52 during Rad51-dependent HR and single-strand annealing (15,21,33,44,47). Human RPA (hRPA) interaction site within hRad52 protein involves species-specific C-terminal region of the Rad52 protein (47) and two similar amino-acid sequences within hRPA, one in the OB fold A, which belongs to the RPA70 subunit and another in the RPA32 subunit (44) (Schematically depicted in Figure 2A). Although acidic cluster region of *Saccharomyces cerevisiae* Rad52 (amino acids 308–311) was reported to be directly involved in RPA binding (48), this region is not conserved in human Rad52 protein. Moreover, no reported mutations within human Rad52 protein specifically disrupt hRad52–hRPA interaction. Amino-acid sequence of the C-terminal region of hRad52 contains a conserved motif found in several hRPA interacting proteins (Figure 2B) (49). Recently, Ciccia *et al.* reported that substitution of conserved RQK motif in human DNA annealing helicase SMARCAL1 (HARP) for AAA significantly reduces its interaction with hRPA protein (50). By analogy with SMARCAL1, we substituted the RQK motif of hRad52 (residues 261–263) for three alanines to construct a hRad52 mutant lacking the capacity to bind hRPA. The resulting mutant protein, hRad52$^{RQK/AAA}$, was expressed and purified along with hRad52$^{1–212}$, which lacks capacity to bind hRPA due to complete deletion of the C-terminal domain responsible for the hRad52-hRPA interaction (Figure 2C). Indeed, deletion of the C-terminal domain yielded hRad52$^{1–212}$ incapable of forming stable complexes with hRPA protein. Similarly, removal of RQK motif significantly reduced interaction between hRad52$^{RQK/AAA}$ mutant and RPA, as evident from the pull-down assays that took advantage of the 6xHistidine tag on hRad52 protein (Figure 2D).

Human RPA allows binding to and wrapping of ssDNA by hRad52, but competes with hRad52$^{RQK/AAA}$ or hRad52$^{1–212}$ for binding

We examined the ability of the two mutants to bind ssDNA in a wrapped configuration and analyzed the effect of hRPA on the wrapping of DNA by hRad52, hRad52$^{RQK/AAA}$ or hRad52$^{1–212}$. These assays were carried out essentially as described above for the wild type protein except that 2 nM hRPA was incubated with ssDNA (1 nM) prior to hRad52 addition. This amount of hRPA should be sufficient to saturate ssDNA considering the subnanomolar affinity of RPA for ssDNA (51–53) and its binding site size of 25–30 nt (54). Indeed under our experimental conditions, hRPA readily bound to short oligonucleotides (Supplementary Figure S4). Approximately 1.5 and 2.5 nM hRPA was sufficient to saturate 1 nM poly(dT)-30 and poly(dT)-60, respectively and twice that concentration required to saturate 2 nM ssDNA. The hRad52-binding trend of an initial increase followed by a decrease in FRET with increasing protein concentration was conserved even in the presence of
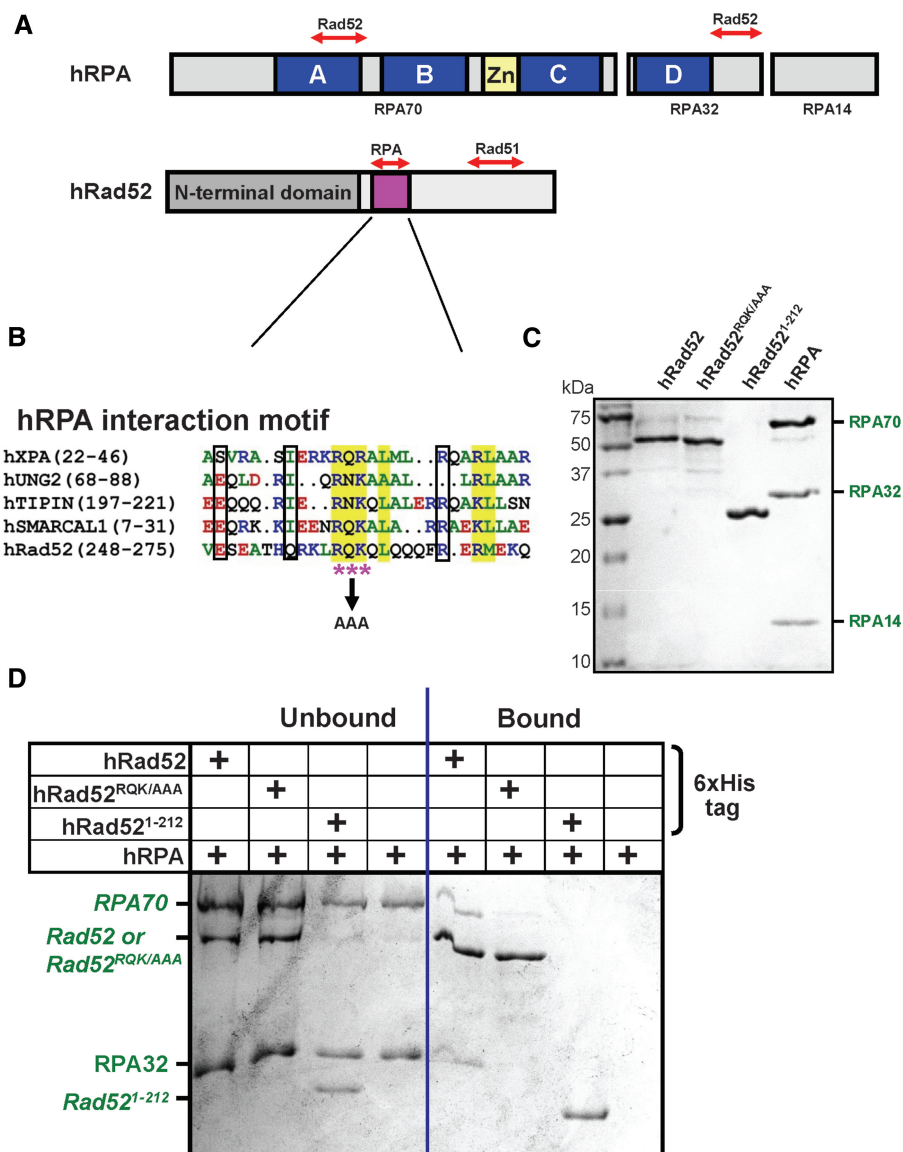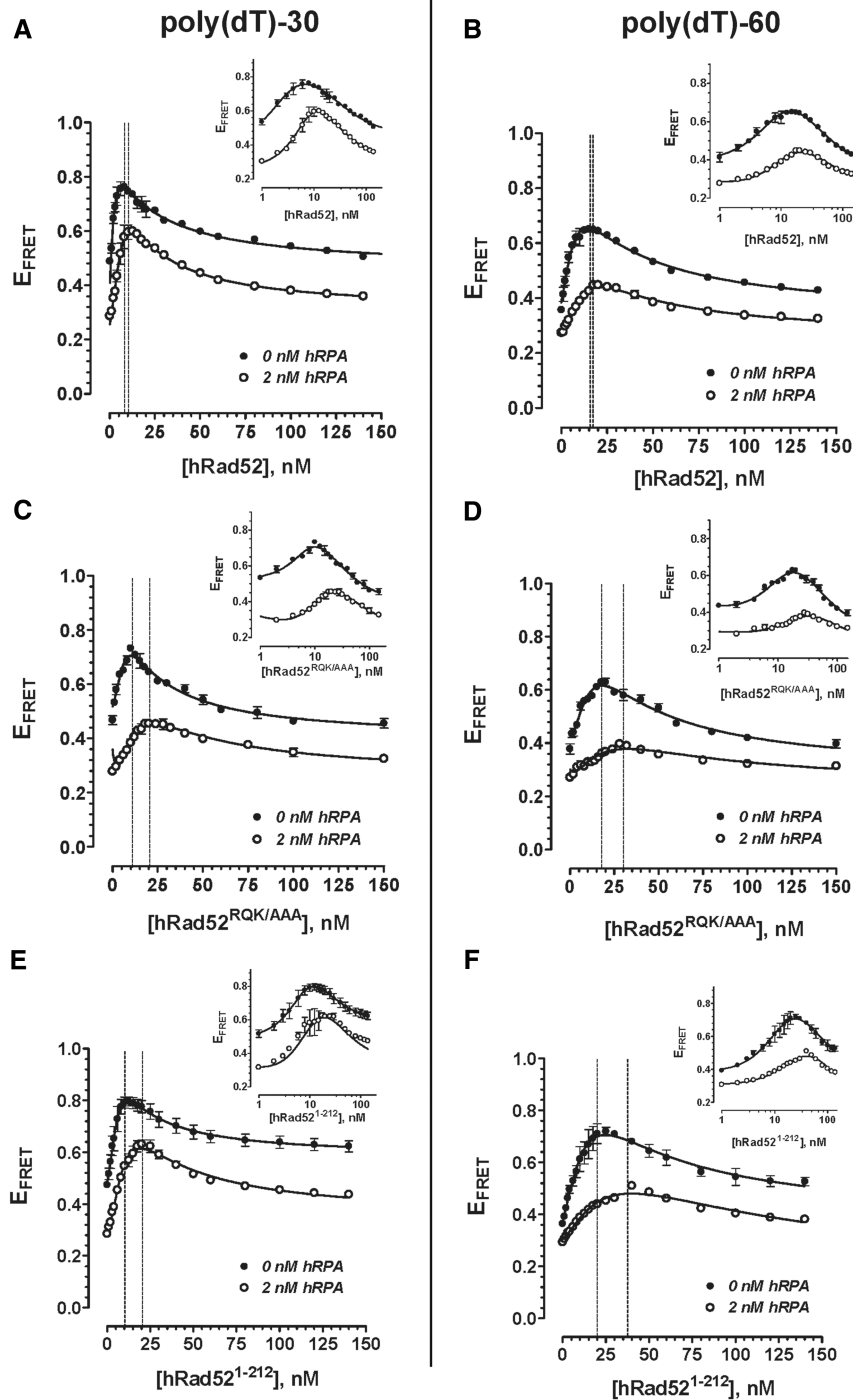
Figure 2. hRad52$^{RQK/AAA}$ and hRad52$^{1-212}$ display impaired interaction with hRPA. (**A**) Schematic representation of hRPA and hRad52 domain organization. Blue boxes in the hRPA70 and RPA32 subunits denoted as A, B, C & D represent 4 OB-fold of hRPA responsible for ssDNA binding. The hRPA interaction region of hRad52 was shown as a pink box. (**B**) Sequence alignment of the putative hRPA-interacting motifs from hRad52, hXPA, hUNG2, hTIPIN and hSMARCAL1. (**C**) SDS–PAGE depicting purified hRad52, hRad52$^{RQK/AAA}$, hRad52$^{1-212}$ and hRPA proteins. (**D**) Pull-down assays using 6xHis-tagged hRad52, hRad52$^{RQK/AAA}$ or hRad52$^{1-212}$ (5 μM) incubated with untagged hRPA (5 μM) and Ni-NTA magnetic beads. Both, unbound and bound fractions are shown as specified in the table above the gel.

hRPA (Figure 3A and B). The starting E_{FRET} value prior to the addition of hRad52 was lower because hRPA-binding straightened the DNA relative to that in the protein-free DNA. Although hRPA had little or no effect on the hRad52 concentration required to achieve maximum E_{FRET} and maximum wrapping of ssDNA, we observed an overall decrease in the E_{FRET} values, suggesting either the inability of hRad52 to fully wrap the hRPA-coated ssDNA or change in the shape of hRad52 oligomer (42,43).

Human Rad52$^{RQK/AAA}$ mutant binds and wraps poly(dT)-30 and poly(dT)-60 in the same manner as does the wild type. We observed the biphasic mode of ssDNA binding with highest E_{FRET} achieved at ~7 nM of

hRad52$^{RQK/AAA}$, suggesting that R^{261}A, Q^{262}A, K^{263}A mutations did not affect the ssDNA binding (Figure 3C and D). In the case of hRad52$^{1-212}$, structural studies revealed the assembly of predominantly 11-membered ring with the overall diameter very similar to that of the 7-membered ring observed for the full length protein (35,36). Similar to the full length protein, the hRad52$^{1-212}$ truncation mutant showed a dual mode of ssDNA binding with the highest E_{FRET} achieved at approximately 10 nM hRad52$^{1-212}$ (close to one undecameric ring) for 30-mer and 20 nM hRad52$^{1-212}$ (two rings) for 60-mer (Figure 3E and F). Human Rad52$^{RQK/AAA}$ and hRad52$^{1-212}$ mutant proteins displayed a similar overall trend of DNA-binding isotherms in the presence of

Figure 3. hRad52$^{RQK/AAA}$ and hRad52$^{1–212}$ but not hRad52 compete with hRPA for binding to ssDNA. Comparison of ssDNA-binding modes observed for hRad52, hRad52$^{RQK/AAA}$ or hRad52$^{1–212}$ in the absence or presence of hRPA. Where indicated, hRPA was added to the ssDNA and an initial E_{FRET} value was measured prior to initiating the protein titration. The calculated E_{FRET} values are plotted against the corresponding protein concentration (nM, monomers). (**A**) The binding isotherms for 1 nM poly(dT)-30 ssDNA binding by hRad52 alone (filled circles), in the presence 2 nM hRPA (open circles). (**B**) Binding of 1 nM poly(dT)-60 by hRad52 alone (closed circles) and 2 nM hRPA (open circles). (**C**) The isotherms for binding of hRad52$^{RQK/AAA}$ to 1 nM poly(dT)-30 ssDNA without hRPA (closed circles) and 2 nM hRPA (open circles). (**D**) The binding isotherms for hRad52$^{RQK/AAA}$ and 1 nM poly(dT)-60 without hRPA (closed circles) and 2 nM hRPA (open circles). (**E**) The isotherms for binding of hRad52$^{1–212}$ to 1 nM poly(dT)-30 ssDNA without hRPA (closed circles) and 2 nM hRPA (open circles). (**F**) The binding isotherms for hRad52$^{1–212}$ and 1 nM poly(dT)-60 without hRPA (closed circles) and 2 nM hRPA (open circles).

hRPA (Figure 3C–F). However, higher hRad52$^{RQK/AAA}$ or hRad52$^{1–212}$ concentrations were required to reach maximum E_{FRET} suggesting that, unlike hRad52, hRad52$^{RQK/AAA}$ and hRad52$^{1–212}$ compete with hRPA for the ssDNA lattice.

The active species during annealing are ssDNA–hRad52(+hRPA) complexes

The investigation into the effects of yeast RPA on Rad52-mediated DNA annealing has demonstrated that RPA is required for Rad52 to anneal long DNA molecules, but interferes with the Rad52-mediated annealing of shorter oligonucleotides (15). However, the precise mechanism of hRad52-mediated annealing, with or without hRPA, remains elusive. For example, it is unknown whether annealing occurs between a hRad52–ssDNA complex and a protein-free ssDNA strand, or could involve two hRad52–ssDNA complexes.

We investigated the ability of hRad52, hRad52$^{RQK/AAA}$ or hRad52$^{1–212}$ to anneal complementary 28-nt DNA strands and how hRPA influences these annealing reactions (Figure 4). The ssDNA molecules were internally labeled with the donor Cy3 (T-28) or the acceptor Cy5 (P-28) such that when the annealed product was formed, the proximity of the dyes to each other (∼5–6 nt) resulted in high E_{FRET} (∼0.81). Each oligonucleotide (0.5 nM in final assays or 1 nM in respective half-reactions) was separately preincubated with hRad52, hRad52$^{RQK/AAA}$, hRad52$^{1–212}$, and/or hRPA proteins. Annealing was initiated by mixing the two half-reactions.

Representative progress curves for annealing mediated by hRad52, hRad52$^{RQK/AAA}$ and hRad52$^{1–212}$ are shown in Figure 4A. The annealing assays performed with a range of hRad52 (Figure 4, left column), hRad52$^{RQK/AAA}$ (middle column) or hRad52$^{1–212}$ concentrations (right column) yielded the initial rates of annealing (Figure 4B) and the annealing extents (fraction of dsDNA, as measured by FRET, when the equilibrium between annealing and duplex melting is achieved under each condition) (Figure 4C). At each concentration tested, hRad52, hRad52$^{RQK/AAA}$ or hRad52$^{1–212}$ were capable of annealing the oligonucleotides, but to different extents. Under our conditions (low ionic strength), the rate and extent of spontaneous annealing of the oligonucleotides in the absence of proteins or in the presence of hRPA alone were negligible. Initially, both the rate and extent of annealing increased with the increasing concentration of hRad52. The fastest annealing was achieved with 8 nM hRad52 (Figure 4B, left). At over-saturating hRad52 concentrations (15–50 nM), the rate of annealing was significantly reduced (Figure 4B, left), but the extent of dsDNA formation remained nearly 100% (Figure 4C, left). Results for hRad52$^{RQK/AAA}$ annealing were consistent with those of the full-length protein with 8 nM being optimal for annealing (Figure 4B and C, middle). The maximum annealing rate of hRad52$^{1–212}$ was reduced by approximately 2-fold relative to the full-length protein suggesting that difference in oligomerization state or lack of whole C-terminal region impairs the ssDNA annealing activity. However, at the optimal protein concentration (10 nM), the extent of annealing reached nearly 100% (Figure 4B and C, right).

The effect of hRPA on the annealing reaction mediated by hRad52, hRad52$^{RQK/AAA}$ or hRad52$^{1–212}$ is also shown in Figure 4. Although annealing still occurred, the presence of hRPA (2 nM) negatively affected both the rate and extent of annealing by hRad52 as indicated by the shallower curve and the lower E_{FRET} values achieved compared to the annealing assays run in the absence of hRPA (Figure 4A–C left column). Over the range of hRad52 concentrations tested in the presence of 2 nM hRPA, the most favorable annealing condition was achieved at 10 nM hRad52 (Figure 4B and C) which is similar to the optimum binding/wrapping concentration of hRad52 in the presence of hRPA (Figure 4D). For adequate comparison, the binding data shown in Figure 4D is an expanded view of the concentrations between 0 and 50 nM hRad52 shown in Figure 3A.

In agreement with observed competition for ssDNA binding, DNA annealing by hRad52$^{RQK/AAA}$ (Figure 4B and C, middle) and hRad52$^{1–212}$ (Figure 4B and C, right) was severely impaired in the presence of hRPA protein. The annealing rate in the presence of optimal concentrations of hRad52$^{RQK/AAA}$ and hRad52$^{1–212}$ decreased approximately 7- and 10-fold respectively, in the presence of hRPA. In contrast, hRPA caused only 4-fold decrease in the annealing rate of the full-length protein.

Human RPA is known to possess a helix destabilization propensity (55). In agreement with published data, addition of hRPA directly to dsDNA (annealed T-28 and P-28 DNA) resulted in a decrease in FRET due to the destabilization of the duplex upon hRPA binding (Supplementary Figure S5A and B). The presence of hRad52 resulted in both slower melting rate and limited extent of melting reaction likely due to two processes that offset each other in equilibrium: annealing by hRad52 protein and hRPA-mediated duplex destabilization, also explaining the reduced extent of hRad52-mediated annealing in the presence of hRPA. Additionally, both hRad52$^{RQK/AAA}$ and hRad52$^{1–212}$ displayed milder inhibitory effect on extent of hRPA-mediated duplex destabilization (Supplementary Figure S5A) and caused no change in the initial rate of duplex melting by hRPA (Supplementary Figure S5B).

DISCUSSION

In the current study, we demonstrated that hRad52 stably binds and wraps both, protein free and hRPA-coated ssDNA.

In the absence of hRPA, the ssDNA concentration yielding the fastest annealing equals the concentration in which the DNA molecules were wrapped around individual hRad52, hRad52$^{RQK/AAA}$ or hRad52$^{1–212}$ rings. Therefore, optimal annealing occurs at conditions in which both strands are bound by hRad52 as opposed to one hRad52–ssDNA complex plus protein-free ssDNA or multi-ringed hRad52–ssDNA complexes interacting with each other.
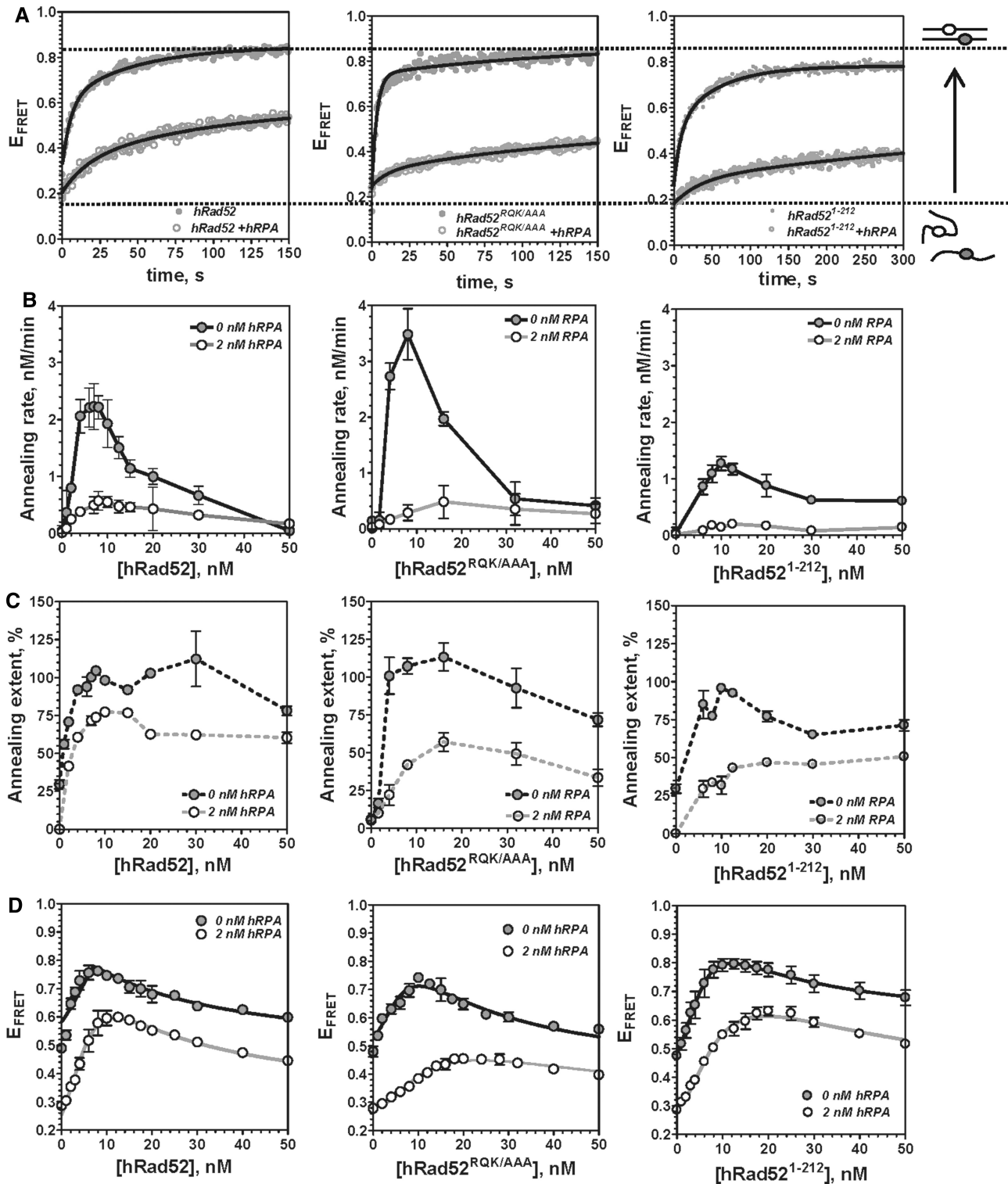
Figure 4. Effects of hRPA on ssDNA binding and annealing by hRad52. FRET-based annealing assays were preformed using 0.5 nM of each, Target-28 and Probe-28 oligonucleotides internally-labeled with Cy3 and Cy5, respectively. (**A**) Representative annealing curves depict reactions with 8 nM hRad52, hRad52$^{RQK/AAA}$ and hRad52$^{1-212}$ in the absence (grey closed circles) or presence of 2 nM hRPA (open circles), conditions most favoring the annealing. Three independent FRET efficiency (E_{FRET}) trajectories were collected and averaged for each condition. The data were fitted to a double exponential to yield the amplitudes of E_{FRET} change at equilibrium. The initial linear increase in the E_{FRET} yielded annealing rates. The E_{FRET} values corresponding to the fully single-stranded and double-stranded DNA are indicated by the dotted lines. The substrates and product of the annealing reaction are schematically depicted on the right of the graph. (**B**) Initial rates of annealing reactions using protein-free ssDNA (grey circles) and RPA-coated ssDNA (open circles) carried out by hRad52, hRad52$^{RQK/AAA}$ and hRad52$^{1-212}$ at the indicated concentrations. (**C**) Extents of the annealing reactions were calculated from the amplitude of E_{FRET} change for each condition. (**D**) The E_{FRET} trends for hRad52, hRad52$^{RQK/AAA}$ and hRad52$^{1-212}$ binding to poly(dT)-30 ssDNA (1 nM) in the absence or presence of hRPA (2 nM) are shown for comparison of optimal binding and annealing conditions.

Similarly, the most efficient annealing and the fastest homology search occurs when hRad52 heptameric rings and hRPA-coated ssDNA are present as stoichiometric complexes. However, the rate and extent of annealing were significantly reduced from those observed in the annealing assays without hRPA.

Moreover, the comparison study of hRad52 with hRad52$^{RQK/AAA}$ or hRad52$^{1-212}$ demonstrated that hRad52–hRPA interaction not only facilitates binding of hRad52 to hRPA-coated ssDNA, but is also important for counteracting helix destabilization activity of hRPA.

The two structures obtained for the ssDNA annealing domain of hRad52 positioned a putative DNA-binding groove around the outer surface of the protein ring (35,36). This proposition was further validated by mutational studies that highlighted the importance of the positively charged residues located in this groove for ssDNA binding (41). The secondary DNA-binding site was proposed to run along the upper rim of the hRad52 ring (37). In yeast, the *in vivo* concentration of Rad52 is $\sim 10^3$ molecules/cell, which would be sufficient to stoichiometrically bind 4 kb of ssDNA (56). With the fluctuating levels of ssDNA during normal cell cycle there would be ample amounts of Rad52 to form Rad52–ssDNA complexes. Under conditions, where a lot of ssDNA is produced due to ongoing recombinational DNA repair, the ratio of Rad52 to ssDNA will result in DNA mostly present in a wrapped configuration, while it would be unlikely to find ssDNA oversaturated with Rad52 during the steps in DNA maintenance and repair requiring Rad52 annealing activity. The search for the region of sufficient complementarity proceeds via continuous interaction between nucleoprotein complexes containing both DNA strands (57). However, little is known about the nature of the complex formed between hRad52 and hRPA-coated ssDNA. Moreover, both ring (58) and non-ring forms of hRad52 protein (42,43) were proposed to act in DNA annealing.

Here, we provide experimental evidence demonstrating that at stoichiometric amounts of protein:DNA, ssDNA is bound around the perimeter of the full-length hRad52 ring. An ssDNA molecule bound around the perimeter of the hRad52 ring would be in a low energy state due to the favorable interactions between the negatively charged phosphodiester backbone and the positively charged residues of the protein. The continuous binding site around the protein ring would position the phosphodiester backbone of the ssDNA within the groove with the bases extending outward (35,36) with each hRad52 protomer-binding 4 nt (35,46). This hRad52–ssDNA conformation would be ideal for probing base pair complementarity of protein-free DNA, DNA coated with hRPA or another hRad52–ssDNA complex (35).

If during hRad52-mediated annealing, a significant number of perfect base pairs are identified so that the equilibrium is shifted toward product formation, then rearrangement of the ssDNA–hRad52 complex would be required to release the DNA strand(s) from one or both rings. It has been proposed that duplex DNA cannot be contained within the narrow DNA-binding groove around

the hRad52 ring without introducing a large conformational change (35). However, it can be accommodated in the secondary-binding site (37). In agreement, we observed that hRad52 is capable of binding and distorting dsDNA, but not to the same degree as ssDNA (Supplementary Figure S3). The maximal FRET signal achieved with dually labeled dsDNA was lower compared to that for ssDNA and was achieved at a higher protein/DNA ratio. This could be either due to the difference in binding mode or affinity between ssDNA and dsDNA.

We observed optimal annealing at hRad52 concentrations in which the DNA strands were wrapped around a single hRad52 ring. At high protein concentrations when multiple hRad52 rings bind to a single ssDNA molecule, the interactions between the DNA backbone and the positively-charged residues of the protein will be maintained, but a sacrifice would be made in the number of contacts between the DNA and each subunit of a bound hRad52 ring. Although this altered DNA binding locally preserves the presentation of the bases, the overall conformation of the multi-ringed hRad52–ssDNA complex suggests that the search for complementary bases would be disrupted, explaining the decrease in the rate of annealing when excess hRad52 is present. Another explanation for the reduced annealing efficiency at higher hRad52 concentrations is the increase in DNA-free hRad52 oligomers. These 'empty' rings would be nonproductive partners for the hRad52–ssDNA complexes. In agreement with this proposition, the rate of annealing was significantly reduced at hRad52 concentrations exceeding 10 nM, while the extent of the reaction remained nearly 100% even at much higher concentrations of the protein.

Human Rad52 displayed similar ssDNA-binding modes even in the presence of hRPA. However, hRad52 did not wrap hRPA-coated ssDNA as completely. It is likely that hRad52 does not displace hRPA from the ssDNA, but rather distorts the ssDNA–hRPA complex. This proposal is supported by the observation that the affinity of the hRPA–hRad52 complex for ssDNA is higher than that observed for the individual proteins separately (44). Although the gel-mobility shift and SPR experiments (44) could not unambiguously determine which species in the hRPA–hRad52 complex actually contacts ssDNA, the C-terminal domain of hRad52 that interacts with hRPA but has no DNA-binding capacity of its own (47) also enhanced hRPA affinity for ssDNA. Therefore, interaction with hRad52 per se does not dislodge hRPA from ssDNA. We can envision that the same fragment of ssDNA can accommodate both proteins, which interact with one another, and that the formation of the hRPA–ssDNA–hRad52 complex may prevent the ssDNA from binding completely within the DNA-binding groove of hRad52. Formation of the hRPA–ssDNA–hRad52 complex on short oligonucleotides that can bind only one or two hRPA molecules distinguishes these proteins from their yeast counterparts, where formation of the stable yRPA–ssDNA–yRad52 complex requires multiple RPA molecules bound to the same ssDNA (59).
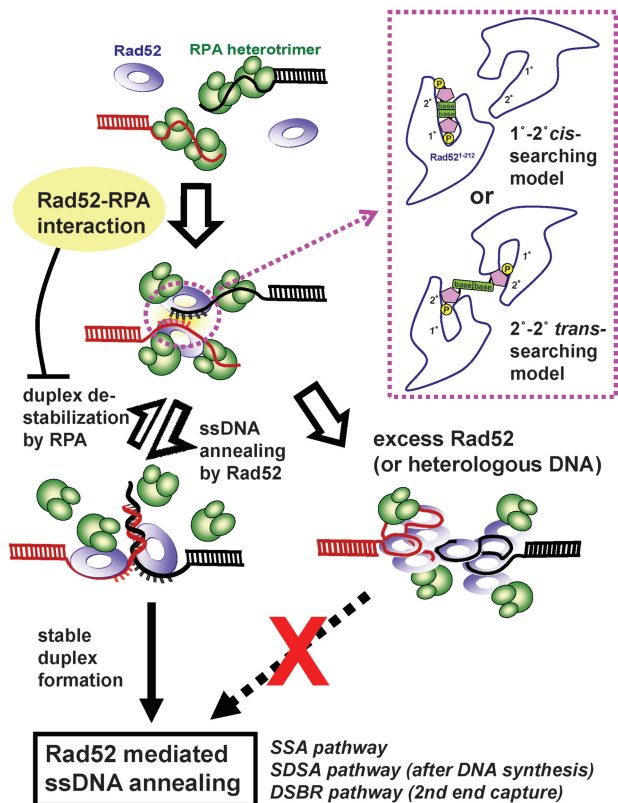
Figure 5. Model for DNA binding and annealing by hRad52 in the presence of hRPA. At optimal protein concentrations, hRad52 binds the ssDNA–hRPA complex through hRad52–hRPA interaction and forms hRad52–hRPA–ssDNA ternary complex in wrapped configuration. This binding mode yields hRad52–hRPA–ssDNA 'active' complexes required for efficient annealing of complementary DNA strands. Due to the presence of two DNA-binding sites in each hRad52 ring, we can envision two possible mechanisms for homology search between hRad52–hRPA–ssDNA complexes (schematically illustrated inside the inset box). Predicted positions of primary and secondary DNA-binding sites are denoted as 1° and 2°. The annealing process is dynamic and is offset by hRPA-mediated duplex destabilization. Excess hRad52 results in multiple hRad52 rings competing for binding to the ssDNA thus forming 'non-active' complexes that inhibit annealing.

The reduced rate and extent of hRad52-mediated annealing in the presence of hRPA may be explained by the competition between hRPA-mediated duplex destabilization and hRad52-mediated annealing. The hRPA heterotrimer contacts ssDNA primarily via the large subunit (RPA70) and occludes ∼30 nt (44,54). As previously stated, human Rad52 was proposed to bind four nt per monomer of the protein ring (35,36,46). Therefore, our 30 nt substrates would ideally permit the complete binding (wrapping) by a single hRPA complex or hRad52 ring. Nevertheless, we observed a more complex binding equilibrium shifting between multiple species including: single hRad52–ssDNA or hRPA–ssDNA complexes, multi-ringed hRad52–ssDNA complexes, or a ternary complex of hRad52–ssDNA–hRPA (Figure 5). It is likely that within this ternary complex, the presence of hRPA is maintained not only by its binding to ssDNA but also by its association with

the C-terminus of hRad52. This would explain the difference in how hRPA affected binding and annealing by hRad52, hRad52$^{RQK/AAA}$ and hRad52$^{1–212}$. Although its equilibrium was shifted due to competition with hRPA, the hRad52$^{RQK/AAA}$ and hRad52$^{1–212}$ mutants bound DNA in a wrapped conformation similar to the full-length protein in the presence of hRPA. However, the addition of hRPA inhibited both the rate and extent of annealing by hRad52$^{RQK/AAA}$ and hRad52$^{1–212}$ to a much greater degree than that of the full-length hRad52 protein. Therefore, the ability of hRad52 to form a complex with hRPA is important for the annealing of complementary DNA because it may facilitate partial release of hRPA from the DNA thus allowing hRad52 to initiate and then successfully complete annealing. The newly formed duplex, however, will be the substrate for hRPA-mediated melting. Hence, the observed rate and extent (which reflects equilibrium between free ssDNA, DNA in a duplex form, bound to hRPA and bound to hRad52) of annealing were lower in the presence of hRPA.

This reduction in the rate of hRad52-mediated annealing of oligonucleotides by hRPA needs to be reconciled with the finding that RPA is required for annealing of plasmid-length DNA by yeast Rad52 (15). Dynamic equilibrium between the binding of hRad52 and hRPA on ssDNA and the effect of hRPA on the annealing ability of hRad52 is necessary to permit the local competition that will ultimately ensure that annealing occurs over complementary regions of sufficient length, and thus will be beneficial for annealing longer stretches of truly homologous DNA as occurs *in vivo*. The binding and annealing trends we observed *in vitro* using oligonucleotides may therefore accurately represent these focused interactions between hRad52 and hRPA on the DNA lattice.

In addition to revealing the preferred geometry of ssDNA involved in the search for complementary sequence, our results have another important implication: the most effective annealing occurs between two hRad52–ssDNA (or hRad52–ssDNA–hRPA) complexes and not between a nucleoprotein complex and a protein-free ssDNA. Although in our model we treat hRad52 oligomers as rings for all steps of binding and annealing, similar model can be drawn for other possible conformations including, for example, open or partially disassembled rings as long as a curved nature of the oligomer is preserved. Because the search for homology occurs without dissociation of the two complexes after the initial pairing event (57), we can envision the annealing process whereby the two hRad52 oligomers interact with one another probing homology until an extended complementary region is found (schematically depicted in the inset in Figure 5). When homology between the two ringed structures is probed 4 nt at a time, a portion of one strand may be pulled out of the deep groove within the ring and temporarily placed into the secondary DNA-binding site of the interacting ring and probed for complementarity. Alternatively, portions of both strands may be moved up to the secondary DNA-binding sites of their respective rings. If the first 4 nt tested on the two

strands are indeed complementary, the resulting duplex formation will promote the probing of the adjacent 4 nt.

SUPPLEMENTARY DATA

Supplementary Data are available at NAR Online.

ACKNOWLEDGEMENTS

The authors would like to thank Dr Robert Pugh for his critical reading of the manuscript.

FUNDING

REFERENCES

1. Sung,P., Krejci,L., Van Komen,S. and Sehorn,M.G. (2003) Rad51 recombinase and recombination mediators. *J. Biol. Chem.*, **278**, 42729–42732.
2. Ivanov,E.L., Sugawara,N., Fishman-Lobell,J. and Haber,J.E. (1996) Genetic requirements for the single-strand annealing pathway of double-strand break repair in Saccharomyces cerevisiae. *Genetics*, **142**, 693–704.
3. Sugawara,N., Wang,X. and Haber,J.E. (2003) In vivo roles of Rad52, Rad54, and Rad55 proteins in Rad51-mediated recombination. *Mol. Cell.*, **12**, 209–219.
4. Symington,L.S. (2002) Role of RAD52 epistasis group genes in homologous recombination and double-strand break repair. *Microbiol. Mol. Biol. Rev.*, **66**, 630–670, table of contents.
5. Bendixen,C., Sunjevaric,I., Bauchwitz,R. and Rothstein,R. (1994) Identification of a mouse homologue of the Saccharomyces cerevisiae recombination and repair gene, RAD52. *Genomics*, **23**, 300–303.
6. Bezzubova,O.Y., Schmidt,H., Ostermann,K., Heyer,W.D. and Buerstedde,J.M. (1993) Identification of a chicken RAD52 homologue suggests conservation of the RAD52 recombination pathway throughout the evolution of higher eukaryotes. *Nucleic Acids Res.*, **21**, 5945–5949.
7. Mortensen,U.H., Bendixen,C., Sunjevaric,I. and Rothstein,R. (1996) DNA strand annealing is promoted by the yeast Rad52 protein. *Proc. Natl Acad. Sci. USA*, **93**, 10729–10734.
8. Muris,D.F., Bezzubova,O., Buerstedde,J.M., Vreeken,K., Balajee,A.S., Osgood,C.J., Troelstra,C., Hoeijmakers,J.H., Ostermann,K., Schmidt,H. *et al.* (1994) Cloning of human and mouse genes homologous to RAD52, a yeast gene involved in DNA repair and recombination. *Mutat. Res.*, **315**, 295–305.
9. Ostermann,K., Lorentz,A. and Schmidt,H. (1993) The fission yeast rad22 gene, having a function in mating-type switching and repair of DNA damages, encodes a protein homolog to Rad52 of Saccharomyces cerevisiae. *Nucleic Acids Res.*, **21**, 5940–5944.
10. Benson,F.E., Baumann,P. and West,S.C. (1998) Synergistic actions of Rad51 and Rad52 in recombination and DNA repair. *Nature*, **391**, 401–404.
11. Shinohara,A. and Ogawa,T. (1998) Stimulation by Rad52 of yeast Rad51-mediated recombination. *Nature*, **391**, 404–407.
12. New,J.H., Sugiyama,T., Zaitseva,E. and Kowalczykowski,S.C. (1998) Rad52 protein stimulates DNA strand exchange by Rad51 and replication protein A. *Nature*, **391**, 407–410.
13. Sung,P. (1997) Function of yeast Rad52 protein as a mediator between replication protein A and the Rad51 recombinase. *J. Biol. Chem.*, **272**, 28194–28197.
14. Mortensen,U.H., Erdeniz,N., Feng,Q. and Rothstein,R. (2002) A molecular genetic dissection of the evolutionarily conserved N terminus of yeast Rad52. *Genetics*, **161**, 549–562.
15. Sugiyama,T., New,J.H. and Kowalczykowski,S.C. (1998) DNA annealing by RAD52 protein is stimulated by specific interaction with the complex of replication protein A and single-stranded DNA. *Proc. Natl Acad. Sci. USA*, **95**, 6049–6054.
16. Couedel,C., Mills,K.D., Barchi,M., Shen,L., Olshen,A., Johnson,R.D., Nussenzweig,A., Essers,J., Kanaar,R., Li,G.C. *et al.* (2004) Collaboration of homologous recombination and nonhomologous end-joining factors for the survival and integrity of mice and cells. *Genes Dev.*, **18**, 1293–1304.
17. Bugreev,D.V., Hanaoka,F. and Mazin,A.V. (2007) Rad54 dissociates homologous recombination intermediates by branch migration. *Nat. Struct. Mol. Biol.*, **14**, 746–753.
18. Miyazaki,T., Bressan,D.A., Shinohara,M., Haber,J.E. and Shinohara,A. (2004) In vivo assembly and disassembly of Rad51 and Rad52 complexes during double-strand break repair. *EMBO J.*, **23**, 939–949.
19. Sugiyama,T., Kantake,N., Wu,Y. and Kowalczykowski,S.C. (2006) Rad52-mediated DNA annealing after Rad51-mediated DNA strand exchange promotes second ssDNA capture. *EMBO J.*, **25**, 5539–5548.
20. McIlwraith,M.J. and West,S.C. (2008) DNA repair synthesis facilitates RAD52-mediated second-end capture during DSB repair. *Mol. Cell.*, **29**, 510–516.
21. Nimonkar,A.V., Sica,R.A. and Kowalczykowski,S.C. (2009) Rad52 promotes second-end DNA capture in double-stranded break repair to form complement-stabilized joint molecules. *Proc. Natl Acad. Sci. USA*, **106**, 3077–3082.
22. Paques,F. and Haber,J.E. (1999) Multiple pathways of recombination induced by double-strand breaks in Saccharomyces cerevisiae. *Microbiol. Mol. Biol. Rev.*, **63**, 349–404.
23. Sugawara,N., Ira,G. and Haber,J.E. (2000) DNA length dependence of the single-strand annealing pathway and the role of Saccharomyces cerevisiae RAD59 in double-strand break repair. *Mol. Cell. Biol.*, **20**, 5300–5309.
24. Lander,E.S., Linton,L.M., Birren,B., Nusbaum,C., Zody,M.C., Baldwin,J., Devon,K., Dewar,K., Doyle,M., FitzHugh,W. *et al.* (2001) Initial sequencing and analysis of the human genome. *Nature*, **409**, 860–921.
25. Stark,J.M., Pierce,A.J., Oh,J., Pastink,A. and Jasin,M. (2004) Genetic steps of mammalian homologous repair with distinct mutagenic consequences. *Mol. Cell. Biol.*, **24**, 9305–9316.
26. Krogh,B.O. and Symington,L.S. (2004) Recombination proteins in yeast. *Annu. Rev. Genet.*, **38**, 233–271.
27. Rijkers,T., Van Den Ouweland,J., Morolli,B., Rolink,A.G., Baarends,W.M., Van Sloun,P.P., Lohman,P.H. and Pastink,A. (1998) Targeted inactivation of mouse RAD52 reduces homologous recombination but not resistance to ionizing radiation. *Mol. Cell. Biol.*, **18**, 6423–6429.
28. Yamaguchi-Iwai,Y., Sonoda,E., Buerstedde,J.M., Bezzubova,O., Morrison,C., Takata,M., Shinohara,A. and Takeda,S. (1998) Homologous recombination, but not DNA repair, is reduced in vertebrate cells deficient in RAD52. *Mol. Cell. Biol.*, **18**, 6430–6435.
29. Yanez,R.J. and Porter,A.C. (2002) Differential effects of Rad52p overexpression on gene targeting and extrachromosomal homologous recombination in a human cell line. *Nucleic Acids Res.*, **30**, 740–748.
30. Lloyd,J.A., Forget,A.L. and Knight,K.L. (2002) Correlation of biochemical properties with the oligomeric state of human rad52 protein. *J. Biol. Chem.*, **277**, 46172–46178.
31. McIlwraith,M.J., Van Dyck,E., Masson,J.Y., Stasiak,A.Z., Stasiak,A. and West,S.C. (2000) Reconstitution of the strand invasion step of double-strand break repair using human Rad51 Rad52 and RPA proteins. *J. Mol. Biol.*, **304**, 151–164.

32. Reddy,G., Golub,E.I. and Radding,C.M. (1997) Human Rad52 protein promotes single-strand DNA annealing followed by branch migration. *Mutat. Res.*, **377**, 53–59.

33. Shinohara,A., Shinohara,M., Ohta,T., Matsuda,S. and Ogawa,T. (1998) Rad52 forms ring structures and co-operates with RPA in single-strand DNA annealing. *Genes Cells*, **3**, 145–156.

34. Stasiak,A.Z., Larquet,E., Stasiak,A., Muller,S., Engel,A., Van Dyck,E., West,S.C. and Egelman,E.H. (2000) The human Rad52 protein exists as a heptameric ring. *Curr Biol*, **10**, 337–340.

35. Singleton,M.R., Wentzell,L.M., Liu,Y., West,S.C. and Wigley,D.B. (2002) Structure of the single-strand annealing domain of human RAD52 protein. *Proc. Natl Acad. Sci. USA*, **99**, 13492–13497.

36. Kagawa,W., Kurumizaka,H., Ishitani,R., Fukai,S., Nureki,O., Shibata,T. and Yokoyama,S. (2002) Crystal structure of the homologous-pairing domain from the human Rad52 recombinase in the undecameric form. *Mol. Cell.*, **10**, 359–371.

37. Kagawa,W., Kagawa,A., Saito,K., Ikawa,S., Shibata,T., Kurumizaka,H. and Yokoyama,S. (2008) Identification of a second DNA binding site in the human Rad52 protein. *J. Biol. Chem.*, **283**, 24264–24273.

38. Pant,K., Shokri,L., Karpel,R.L., Morrical,S.W. and Williams,M.C. (2008) Modulation of T4 gene 32 protein DNA binding activity by the recombination mediator protein UvsY. *J. Mol. Biol.*, **380**, 799–811.

39. Kumar,J.K. and Gupta,R.C. (2004) Strand exchange activity of human recombination protein Rad52. *Proc. Natl Acad. Sci. USA*, **101**, 9562–9567.

40. Henricksen,L.A., Umbricht,C.B. and Wold,M.S. (1994) Recombinant replication protein A: expression, complex formation, and functional characterization. *J. Biol. Chem.*, **269**, 11121–11132.

41. Lloyd,J.A., McGrew,D.A. and Knight,K.L. (2005) Identification of residues important for DNA binding in the full-length human Rad52 protein. *J. Mol. Biol.*, **345**, 239–249.

42. Deng,X., Prakash,A., Dhar,K., Baia,G.S., Kolar,C., Oakley,G.G. and Borgstahl,G.E. (2009) Human replication protein A-Rad52-single-stranded DNA complex: stoichiometry and evidence for strand transfer regulation by phosphorylation. *Biochemistry*, **48**, 6633–6643.

43. Erler,A., Wegmann,S., Elie-Caille,C., Bradshaw,C.R., Maresca,M., Seidel,R., Habermann,B., Muller,D.J. and Stewart,A.F. (2009) Conformational adaptability of Redbeta during DNA annealing and implications for its structural relationship with Rad52. *J. Mol. Biol.*, **391**, 586–598.

44. Jackson,D., Dhar,K., Wahl,J.K., Wold,M.S. and Borgstahl,G.E. (2002) Analysis of the human replication protein A:Rad52 complex: evidence for crosstalk between RPA32, RPA70, Rad52 and DNA. *J. Mol. Biol.*, **321**, 133–148.

45. de Vries,F.A., Zonneveld,J.B., de Groot,A.J., Koning,R.I., van Zeeland,A.A. and Pastink,A. (2007) Schizosaccharomyces pombe Rad22A and Rad22B have similar biochemical properties and form multimeric structures. *Mutat. Res.*, **615**, 143–152.

46. Parsons,C.A., Baumann,P., Van Dyck,E. and West,S.C. (2000) Precise binding of single-stranded DNA termini by human RAD52 protein. *EMBO J.*, **19**, 4175–4181.

47. Park,M.S., Ludwig,D.L., Stigger,E. and Lee,S.H. (1996) Physical interaction between human RAD52 and RPA is required for homologous recombination in mammalian cells. *J. Biol. Chem.*, **271**, 18996–19000.

48. Plate,I., Hallwyl,S.C., Shi,I., Krejci,L., Muller,C., Albertsen,L., Sung,P. and Mortensen,U.H. (2008) Interaction with RPA is necessary for Rad52 repair center formation and for its mediator activity. *J. Biol. Chem.*, **283**, 29077–29085.

49. Mer,G., Bochkarev,A., Gupta,R., Bochkareva,E., Frappier,L., Ingles,C.J., Edwards,A.M. and Chazin,W.J. (2000) Structural basis for the recognition of DNA repair proteins UNG2, XPA, and RAD52 by replication factor RPA. *Cell*, **103**, 449–456.

50. Ciccia,A., Bredemeyer,A.L., Sowa,M.E., Terret,M.E., Jallepalli,P.V., Harper,J.W. and Elledge,S.J. (2009) The SIOD disorder protein SMARCAL1 is an RPA-interacting protein involved in replication fork restart. *Genes Dev.*, **23**, 2415–2425.

51. Gomes,X.V., Henricksen,L.A. and Wold,M.S. (1996) Proteolytic mapping of human replication protein A: evidence for multiple structural domains and a conformational change upon interaction with single-stranded DNA. *Biochemistry*, **35**, 5586–5595.

52. Gomes,X.V. and Wold,M.S. (1996) Functional domains of the 70-kilodalton subunit of human replication protein A. *Biochemistry*, **35**, 10558–10568.

53. Kim,C., Snyder,R.O. and Wold,M.S. (1992) Binding properties of replication protein A from human and yeast cells. *Mol. Cell. Biol*, **12**, 3050–3059.

54. Kim,C., Paulus,B.F. and Wold,M.S. (1994) Interactions of human replication protein A with oligonucleotides. *Biochemistry*, **33**, 14197–14206.

55. Lao,Y., Lee,C.G. and Wold,M.S. (1999) Replication protein A interactions with DNA. 2. Characterization of double-stranded DNA-binding/helix-destabilization activities and the role of the zinc-finger domain in DNA interactions. *Biochemistry*, **38**, 3974–3984.

56. Ghaemmaghami,S., Huh,W.K., Bower,K., Howson,R.W., Belle,A., Dephoure,N., O'Shea,E.K. and Weissman,J.S. (2003) Global analysis of protein expression in yeast. *Nature*, **425**, 737–741.

57. Rothenberg,E., Grimme,J.M., Spies,M. and Ha,T. (2008) Human Rad52-mediated homology search and annealing occurs by continuous interactions between overlapping nucleoprotein complexes. *Proc. Natl Acad. Sci. USA*, **105**, 20274–20279.

58. Van Dyck,E., Stasiak,A.Z., Stasiak,A. and West,S.C. (2001) Visualization of recombination intermediates produced by RAD52-mediated single-strand annealing. *EMBO Rep.*, **2**, 905–909.

59. Sugiyama,T. and Kantake,N. (2009) Dynamic regulatory interactions of Rad51, Rad52, and replication protein-A in recombination intermediates. *J. Mol. Biol.*, **390**, 45–55.